Isomeric yield ratios in proton-, ^{3}He-, and α-particle-induced reactions on ^{197}Au

Y. Nagame,[a] K. Sueki,[b] S. Baba,[a] and H. Nakahara[b]
[a]*Department of Radioisotopes, Japan Atomic Energy Research Institute, Tokai-mura, Ibaraki 319-11, Japan*
[b]*Department of Chemistry, Faculty of Science, Tokyo Metropolitan University, Setagaya-ku, Tokyo 158, Japan*
(Received 30 October 1989)

Excitation functions and mean projected recoil-ion ranges of the isomeric nuclei produced in proton-, ^{3}He-, and α-particle-induced reactions on ^{197}Au were measured by an activation technique for bombarding energies $E_p \lesssim 50$ MeV, and $E_{^3\mathrm{He},\alpha} \lesssim 40$ MeV. Isomeric yield ratios (σ_m/σ_g) were determined as a function of the incident particle energy. The experimental excitation functions and isomeric yield ratios were compared with those from statistical model calculations based on the Hauser-Feschbach formalism. From the analysis of excitation functions, recoil-ion ranges, and isomeric yield ratios, the observed reactions were able to be grouped into three distinctly different ones in the energy region studied: (i) compoundlike reaction for $(p,3n)$, $(^3\mathrm{He},4n)$, $(\alpha,3n)$, and $(p,pn)^{196}\mathrm{Au}^m$, (ii) one-neutron stripping reaction for $(^3\mathrm{He},2p)$, and (iii) nonequilibrium one-neutron knockout or pickup reactions with transfer of a small amount of angular momentum for the $(^3\mathrm{He},\alpha)$, $(\alpha,\alpha n)$, and $(p,pn)^{196}\mathrm{Au}^g$ that are intermediate between (i) and (ii). We propose a semiempirical method which predicts isomeric yield ratios in the compoundlike reactions, within a factor of 0.7 to 1.4, from the spin distribution of the compound nucleus.

I. INTRODUCTION

According to the theory of compound-nuclear reaction, residual nuclei are formed as a result of evaporation of light particles from a compound nucleus. If the residual nucleus has a low-lying isomeric state whose spin differs significantly from that of the ground state, the relative population of the isomeric and ground states is determined by the initial excitation energy and spin distribution of the compound nucleus, and the number and the type of emitted particles that carry away energy and angular momentum. Deexcitation of the residual nucleus by γ-ray emission finally determines how the two states are populated.[1,2] The cross section ratio of isomeric pairs (σ_m/σ_g) has been measured to study the level density and the discrete level structure of the residual nucleus.[3–7] The σ_m/σ_g ratio also allows an estimation of the amount of angular momentum transferred into the entrance channel over a wide range of the incident particle energy.[8–14] Recently, an attempt has been made to qualitatively explain σ_m/σ_g for some reactions with considerable preequilibrium contributions.[7,15–23]

The aim of the present work is to study reaction mechanisms by the observation of excitation functions and mean projected recoil-ion ranges of high-spin (m) and low-spin (g) isomers produced in the reactions induced by proton, ^{3}He and α particles on ^{196}Au. In particular, we pay attention to the difference in the isomeric yield ratios between the products of the same final spins and parities; (i) $^{196}\mathrm{Tl}^{m,g}(7^+,2^-)$ and $^{198}\mathrm{Tl}^{m,g}(7^+,2^-)$ produced by the processes of neutron emission, $(^3\mathrm{He},4n)$ and $(\alpha,3n)$ reactions, and (ii) $^{196}\mathrm{Au}^{m,g}(12^-,2^-)$ and $^{198}\mathrm{Au}^{m,g}(12^-,2^-)$ produced by the charged particle emission, $(^3\mathrm{He},2p)$, (p,pn), $(^3\mathrm{He},\alpha)$, and $(\alpha,\alpha n)$ reactions. Also studied are $^{195}\mathrm{Hg}^{m,g}(13/2^+,1/2^-)$ produced by the $(p,3n)$ reaction. Observed excitation functions and isomeric yield ratios are compared with a statistical-model calculation. The recoil-ion ranges are compared with those expected for the full linear momentum transfer. Dependence of isomeric yield ratios on the incident particle energy and the angular momentum in the entrance channel is discussed. A simple method to estimate isomeric yield ratios from the spin distribution of the compound nucleus is proposed for the σ_m/σ_g ratios produced by the compound nuclear process.

II. EXPERIMENTAL PROCEDURES

The excitation functions were obtained by the stacked-foil technique. The mean recoil-ion ranges projected to the beam direction were measured by the thick target-thick catcher-foil method. The target assembly was constructed with ^{197}Au foils (5–10 mg/cm^2 thick) and Al catcher foils (about 10 mg/cm^2) placed downstream of the beam. An Al energy degrader of an appropriate thickness was also inserted in the target assembly.

The proton bombardment was carried out using a cyclotron of the INS (Institute for Nuclear Study, University of Tokyo) with an initial energy of 50 MeV, and the ^{3}He and α bombardments were performed at the RIKEN (Institute of Physical and Chemical Research) cyclotron at 40 MeV. The average beam current, monitored with a Faraday cup connected to a current integrator, was typically about 0.5 electrical μA. The energy-range data of Williamson *et al.*[24] were used to estimate the particle energy at the half-thickness of each target foil.

After bombardment, the γ rays of Tl isotopes were directly measured with a Ge(Li) detector. For Hg and Au isotopes, γ-ray spectrometry was carried out after an appropriate chemical separation.[25] The cross section for a given reaction was evaluated from the sum of the radioactivity of the product nuclei observed in the target and the catcher foil. The product was identified from the

TABLE I. Relevant nuclear properties used in this work.

Nuclides	J^{π}	Half-life	γ-ray energy (keV)	Intensity
$^{198}Tl^{m}$	7^{+}	1.87 h	587.2	0.52
$^{198}Tl^{g}$	2^{-}	5.3 h	675.8	0.108
$^{196}Tl^{m}$	7^{+}	1.41 h	695.4	0.905
$^{196}Tl^{g}$	2^{-}	1.84 h	610.6	0.164
$^{195}Hg^{m}$	$\frac{13}{2}^{+}$	40 h	261.8	0.341
$^{195}Hg^{g}$	$\frac{1}{2}^{-}$	9.5 h	207.1	0.0175
$^{198}Au^{m}$	12^{-}	2.27 d	180.3	0.52
$^{198}Au^{g}$	2^{-}	2.696 d	411.8	0.947
$^{196}Au^{m}$	12^{-}	9.7 h	147.8	0.446
$^{196}Au^{g}$	2^{-}	6.18 d	355.7	0.88

γ-ray energy and half-life. The nuclear data[26,27] used for the evaluation of cross sections are summarized in Table I. The uncertainties in the determined cross sections, recoil-ion ranges, and isomeric yield ratios were estimated to be 10–20% based on the uncertainties associated with the current integration measured with a Faraday cup (2%), target thickness (2%), detector efficiency (3%), γ-ray peak analysis (5–15%) and chemical yield (10%). The uncertainty of the incident particle energy is within the size of the symbol shown in Figs. 1–7.

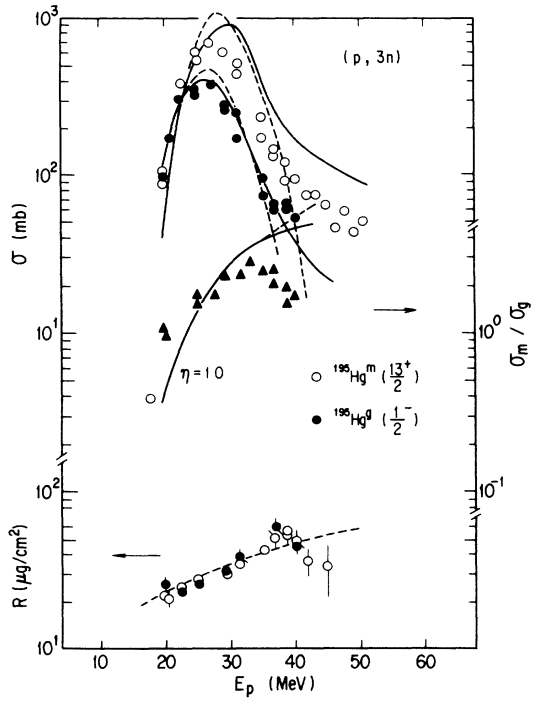

FIG. 1. Excitation functions (upper), mean projected recoil-ion ranges (bottom), and isomeric yield ratio (middle) for the $^{197}Au(p,3n)^{195}Hg^{m,g}$ reactions. Solid and open circles, and solid triangles represent the experimental data. The dashed lines in the upper and middle parts give the results of the compound nucleus-model calculations. The theoretical predictions for the preequilibrium process in combination with the compound nucleus model are indicated by solid lines. The dashed line in the bottom part indicates the predicted recoil-ion ranges for the full linear momentum transfer (see text).

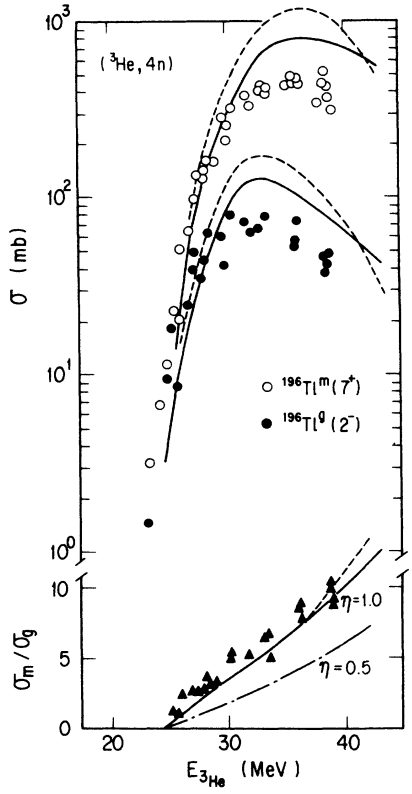

FIG. 2. Same as Fig. 1 for the $^{197}Au(^{3}He,4n)^{196}Tl^{m,g}$ reactions, but there are no recoil-ion range data. Results (σ_m/σ_g) of model calculations with the preequilibrium model using two η values are shown (see text).

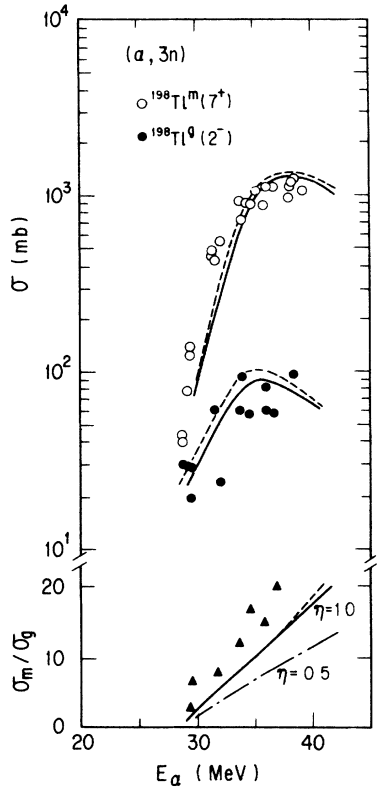

FIG. 3. Same as Fig. 2 for the ^{197}Au(α,3n)^{198}Ti^{m,g} reactions.

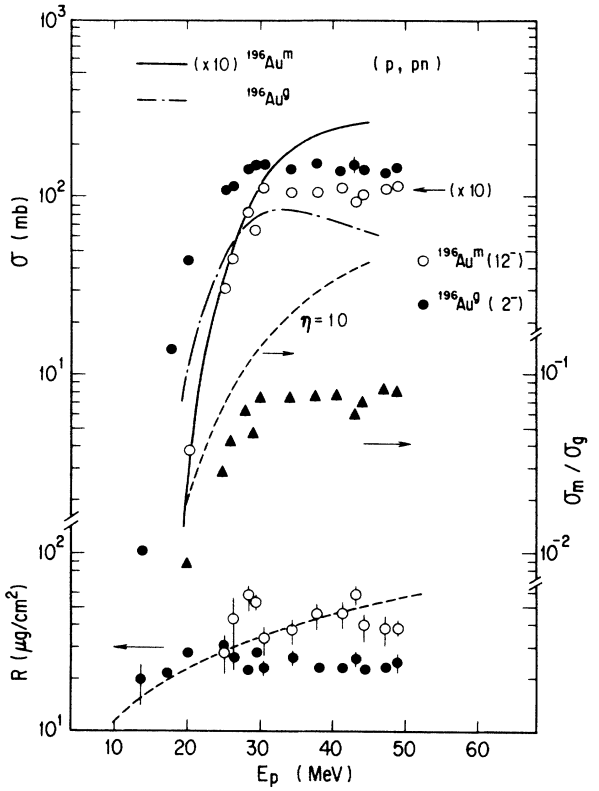

FIG. 5. Same as Fig. 4 for the ^{197}Au(p,pn)^{196}Au^{m,g} reactions.

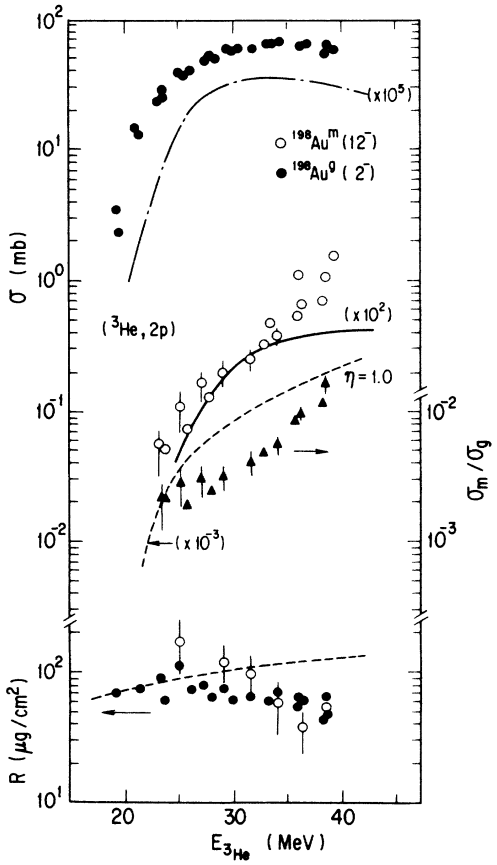

FIG. 4. Same as Fig. 1 for the ^{197}Au(^{3}He,2p)^{196}Au^{m,g} reactions, but the solid and dashed-dotted lines in the upper, and the dashed line in the middle show the calculation with the pre-equilibrium process.

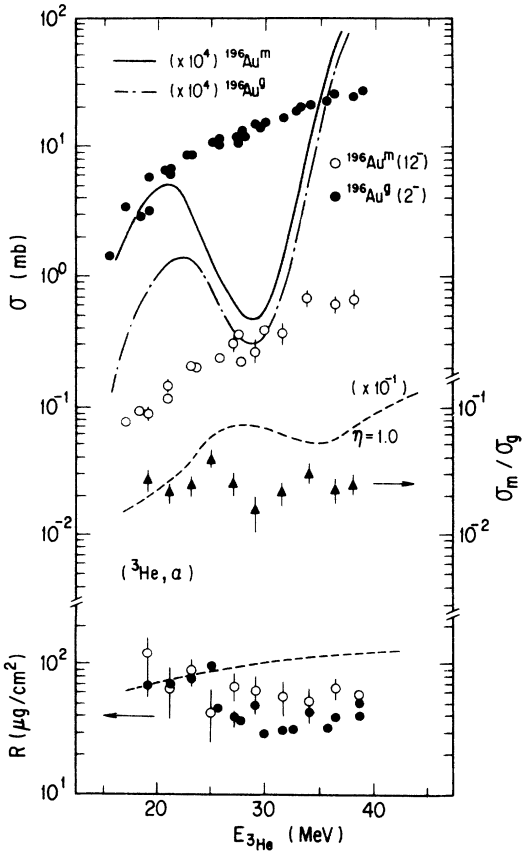

FIG. 6. Same as Fig. 4 for the ^{197}Au(^{3}He,α)^{196}Au^{m,g} reactions.

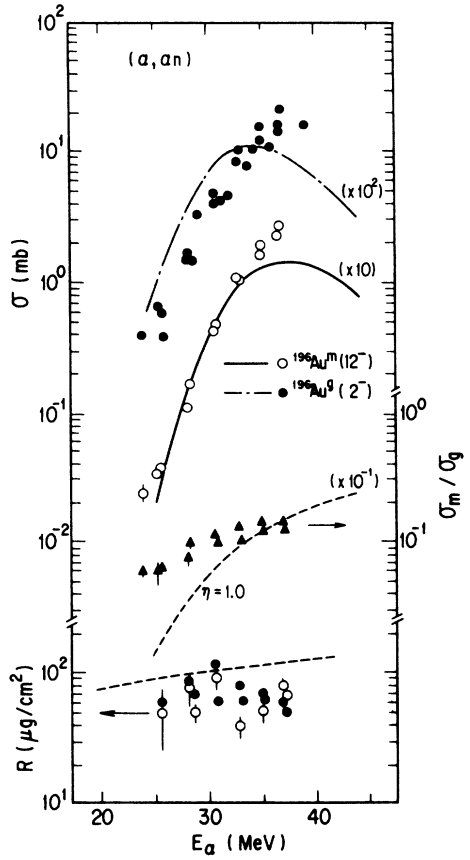

FIG. 7. Same as Fig. 4 for the ^{197}Au$(\alpha,\alpha n)^{198}$Au^{m,g} reactions.

III. STATISTICAL-MODEL CALCULATIONS

Theoretical cross sections and isomeric yield ratios were calculated by using the computer code STAPRE.[23] The reaction is assumed to proceed by, at first, a preequilibrium particle-emission process, which is calculated with the exciton model,[28,29] followed by the evaporation of particles and γ rays. The evaporation was treated by the Hauser-Feshbach formalism[30] based on the angular momentum and parity conservation. As the exciton model, however, does not include the effect of angular momentum, the cross sections of the high-spin and low-spin states were calculated by assuming the spin distribution of the compound nucleus for the residual nucleus formed after the nonequilibrium emission of proton or neutron.

The parameters employed in the model calculation are generally accepted ones.[23] For the transmission coefficient T_l of neutrons, the optical-model parameters of the Wilmore and Hodgson potential[31] were used. For proton, ^{3}He, and α particles, the optical parameters were used from Refs. 32–34. The T_l for γ rays with transition energy ϵ_γ is expressed by the γ-ray strength function $f_{XL}(\epsilon_\gamma)$ for the multipole radiation of type XL. For the $E1$-strength function, the Brink-Axel[35] model was used, and for $M1$, $E2$, $M2$, $E3$, and $M3$ radiations, the Weisskopf model[36] was used.

The mass table reported by Wapstra and Audi[37] was used for the calculation of particle-separation energies. For energies, spins, and parities of the discrete levels of the residual nuclei, the lowest 7 to 15 levels in Ref. 38 were used. The level-density formalism of the back-shifted Fermi gas model expressed by Lang[38] was used for the continuum excitation energy region. The pairing correction in the level density was carried out by using the method of Gilbert and Cameron.[40] The level-density parameter $a = A/10$ was used for all nuclei, where A is the mass number of the nucleus. The spin distribution of the level density is characterized by the effective moment of inertia Θ_{eff}, or by its ratio to the rigid body moment of inertia Θ_{rig} ($\eta=\Theta_{\text{eff}}/\Theta_{\text{rig}}$). The calculations were performed with $\eta=0.5$ and 1.0.[41]

In the calculation of the preequilibrium emission of particles, the following parameters were used. For the initial exciton configurations (p_0,h_0), we used the global parameters[42] (2,1) for proton and (4,0) for α particles. In the case of the ^{3}He induced reactions, the configuration (3,0) taken from the semiempirical systematics[43] was used. The transition rates were calculated by the formula of the Williams and Cline model.[44,45] The average residual two-body matrix element M that appears in the rate formula is expressed as[42]

$$M^2=KA^{-3}E^{-1}, \tag{1}$$

where E is the excitation energy of the composite system. The quantity K is a constant with the dimension of MeV^3, and generally treated as a free parameter[21,42,46] to get a good fit to the experimental data. The K values were fixed as; $K=400$ MeV^3 for proton induced reactions,[46,47] and $K=725$ MeV^3 for ^{3}He and α particles induced reactions.[42]

IV. RESULTS AND DISCUSSION

A. Experimental results and discussion

The excitation functions of the products are shown in the upper parts of Figs. 1 to 7. Reaction types were assigned from the threshold energies and Coulomb barriers in exit channels. The isomeric yield ratios (σ_m/σ_g) are depicted as a function of the incident particle energy in the middle parts of Fig. 1 and Figs. 4–7, and in the lower parts of Figs. 2 and 3. The mean recoil-ion ranges (R) were evaluated by the following equation and plotted in the bottom part of each figure, except for Figs. 2 and 3:

$$R=N_C\cdot T/(N_C+N_T), \tag{2}$$

where N_C is the number of recoil atoms escaping into the catcher foil, N_T the number of atoms remaining in the target, and T the target thickness. The dashed curves for recoil-ion ranges represent the theoretical ranges expected for the full-linear-momentum transfer process. The range-energy calculation was carried out using the Lindhard-Shaff-Schiott (LSS)[48] theory with the relationship of $\rho=3.06\epsilon$, where ρ and ϵ are the dimensionless

quantities corresponding to range and energy, respectively. The recoil range R projected to the beam direction is expressed by the full-momentum transfer range R_0 as follows:[49] (i) for isotropic particle emission

$$R = R_0 \left[1 + \frac{2}{3}\frac{E_{\text{out}}}{E_{\text{in}}} - \frac{1}{15}\frac{E_{\text{out}}^2}{E_{\text{in}}^2} \right], \quad (3)$$

and (ii) for particle emission into the forward direction only

$$R = R_0 \left[1 - \left[\frac{E_{\text{out}}}{E_{\text{in}}} \right]^{1/2} \right]^2, \quad (4)$$

where E_{in} is the kinetic energy of the incident particle and E_{out} the average kinetic energy of the outgoing particle. If the observed R is smaller than R_0, the forward particle emission is favored, as E_{in} is generally larger than E_{out}.

The shapes of excitation functions of the $(p,3n)^{195}\text{Hg}^{m,g}$ reactions below $E_p \sim 40$ MeV (Fig. 1) are typical of the compound nuclear reactions. The slight high-energy tail above $E_p \sim 40$ MeV indicates the contribution of a nonequilibrium process. The recoil-ion ranges for $E_p \lesssim 40$ MeV lie on the dashed curve. The isomeric yield ratio increases with the incident particle energy up to about 35 MeV, and decreases beyond that energy.

Figures 2 and 3 show the excitation functions and the isomeric yield ratios for the $(^3\text{He},4n)^{196}\text{Tl}^{m,g}$ and $(\alpha,3n)^{198}\text{Tl}^{m,g}$ reactions, respectively. The present excitation functions agreed with those reported in Refs. 50–54. The σ_m/σ_g ratios monotonously increase with the incident energy in these two reactions.

It is noted that the excitation functions for the $(^3\text{He},2p)^{198}\text{Au}^{m,g}$ are quite different as shown in Fig. 4. The shape of the excitation function for the low-spin state nucleus $^{198}\text{Au}^g$ indicates that the reaction is of the nature of either direct or nonequilibrium reaction, the cross sections being insensitive to the incident energy after the sharp rise from the threshold. On the other hand, the excitation function of the high-spin state $^{198}\text{Au}^m$ increases with the incident particle energy. The isomeric yield ratio increases with the incident ^{3}He energy. These $\sigma_m(12^-)/\sigma_g(2^-)$ ratios are three orders of magnitude smaller than the $\sigma_m(7^+)/\sigma_g(2^+)$ ratios observed in the compoundlike reactions shown in Figs. 2 and 3. From the above discussion and from the short recoil-ion ranges, it is likely that the $(^3\text{He},2p)$ reaction is a direct one-neutron stripping process.

Excitation functions of both the $(p,pn)^{196}\text{Au}^{m,g}$ reactions in Fig. 5 are similar to those expected for nonequilibrium reactions. There can be contribution of a pickup reaction (p,d), especially in the production of $^{196}\text{Au}^g$. However, a significant difference in the recoil ion range between the products of high-spin state $^{196}\text{Au}^m$ $(J^\pi = 12^-)$ and low-spin state $^{196}\text{Au}^g(J^\pi = 2^-)$ is observed. The recoil-ion range of the nucleus $^{196}\text{Au}^m$ agrees with that expected for the full linear momentum transfer reaction, while that of the low-spin product $^{196}\text{Au}^g$ reveals smaller contribution of linear momentum transfer. The ratio σ_m/σ_g increases with the incident particle energy, and becomes constant beyond $E_p \sim 30$ MeV.

In the case of the ^{3}He induced reaction that produces $^{196}\text{Au}^{m,g}$ (Fig. 6), cross sections steadily increase with the incident energy. The short recoil-ion ranges for $^{196}\text{Au}^{m,g}$ indicate incomplete momentum transfer. The larger mean ranges for the high-spin state $^{196}\text{Au}^m$ above $E_{^3\text{He}} \gtrsim 25$ MeV indicates that the production of $^{196}\text{Au}^m$ becomes feasible only by a greater momentum transfer compared with that of the low-spin state $^{196}\text{Au}^g$. Although the degrees of linear momentum transfer are different between the isomeric pairs, the incident energy dependences of the cross section are similar between the isomers and the σ_m/σ_g ratios are rather insensitive to the incident particle energy. The contribution of the compoundlike $(^3\text{He},2p2n)$ reaction that competes with $(^3\text{He},\alpha)$ is negligible judging from the recoil-ion range and the theoretical calculation discussed below.

The excitation functions, isomeric yield ratios, and recoil-ion ranges for the $(\alpha,\alpha n)^{196}\text{Au}^{m,g}$ reactions are shown in Fig. 7. The $(\alpha,\alpha n)^{196}\text{Au}^g$ reaction was understood as a neutron pickup direct reaction process from the shape of the excitation function and the short recoil-ion ranges.[52,54] Although the measured excitation functions and recoil-ion ranges are limited up to $E_\alpha \sim 40$ MeV, a similar trend is observed in the present study; the cross sections sharply increase with the incident energy up to $E_\alpha \sim 40$ MeV, and the recoil-ion ranges slightly decrease with the incident energy. No significant difference in the mean recoil-ion ranges between $^{196}\text{Au}^m$ and $^{196}\text{Au}^g$ is observed. The σ_m/σ_g ratio gradually increases with the incident energy from 6×10^{-2} to 1.5×10^{-1}.

In Fig. 8, the isomeric yield ratios are summarized as a function of the incident particle energy for various reactions of ^{197}Au. The σ_m/σ_g ratios for the $^{197}\text{Au}+d$ and $^{197}\text{Au}+t$ reactions are taken from Ref. 55. As shown in this figure, the reactions via the compound nucleus formation followed by multiple neutron emission give large isomeric yield ratios $(\sigma_m/\sigma_g \gtrsim 10^{-1})$ compared with those of directlike reaction $(\sigma_m/\sigma_g \lesssim 10^{-1})$. The trend of decreasing σ_m/σ_g ratios at the higher energy in the $(d,2n)$ and $(p,3n)$ reactions may indicate increased contribution of the nonequilibrium process.

In the $(^3\text{He},2p)$ and (d,p) reactions, the isomeric yield ratios are extremely small $(\sigma_m/\sigma_g \lesssim 10^{-2})$. If the neutron particle states of ^{198}Au are populated by a one-step direct reaction, the isomeric yield ratios should strongly depend on the transferred angular momentum and the reaction Q value. In Fig. 9, the σ_m/σ_g ratios are plotted as a function of the incident particle energy per nucleon E/A. One can see that the correlation between σ_m/σ_g and E/A in the two reactions are quite similar. We consider that the observed $(^3\text{He},2p)$ reaction is essentially a one-step neutron stripping reaction similar to the (d,p) reaction.

The isomer ratios in the reactions (p,pn), $(\alpha,\alpha n)$, and $(^3\text{He},\alpha)$ are within the range of 1.5×10^{-2} to 1.5×10^{-1}, and the last one is rather insensitive to the incident particle energy. These reactions of one-neutron pickup or one charged particle and one neutron emission may proceed

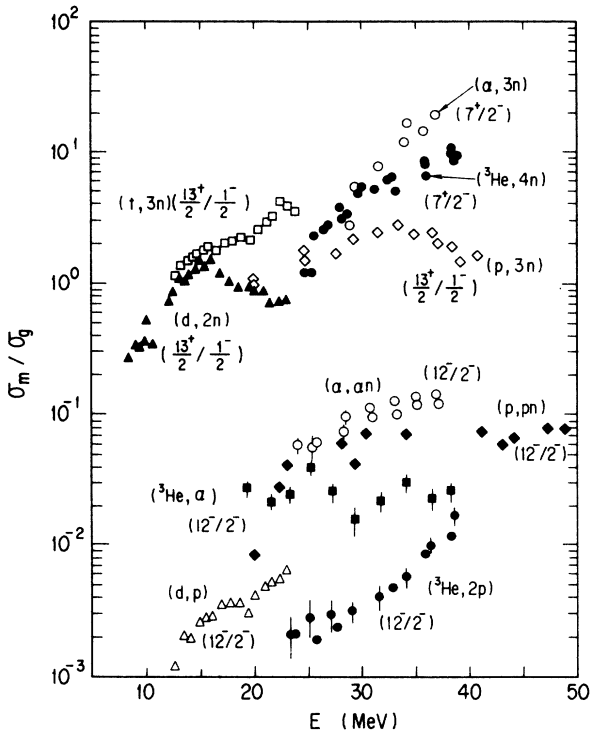

FIG. 8. Isomeric yield ratios as a function of the incident particle energy for the various reactions of ^{197}Au. The data for the ^{197}Au+d and ^{197}Au+t reactions are taken from Ref. 55.

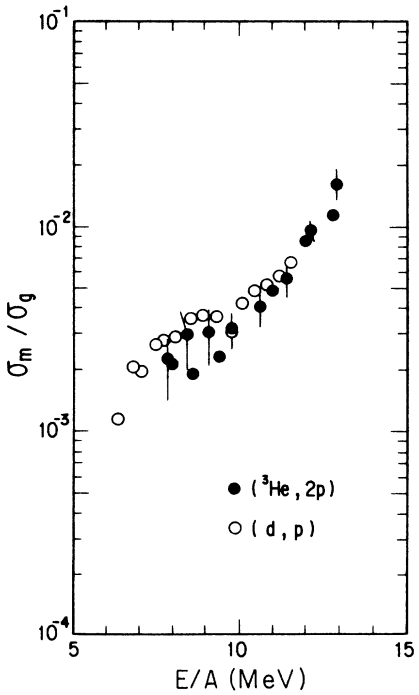

FIG. 9. Relationship between isomeric yield ratio and the incident particle energy per nucleon E/A in the one-step direction reaction processes ^{197}Au(^{3}He,2p)^{198}Au^{m,g} and ^{197}Au(d,p)^{198}Au^{m,g}.

through some intermediate reaction process between the compound nuclear reaction and the one step direct reaction as revealed from the magnitude of the isomeric yield ratios.

B. Comparison of experimental cross section with calculated values

The results of the model calculation are plotted in Figs. 1–7. The excitation functions for the (p,3n), (^{3}He,4n), and (α,3n) reactions are relatively well reproduced by the calculation. The isomeric yield ratio is expected to depend strongly on Θ_{eff}. A better agreement was achieved with $\eta=1.0$ for the (^{3}He,4n) and (α,3n) reactions as shown in Figs. 2 and 3. The trend of the slight high-energy tail of the excitation function observed in the (p,3n) reaction is reproduced by the inclusion of the preequilibrium calculation. However, the feature of decreasing σ_m/σ_g at $E_p \gtrsim 35$ MeV in the (p,3n) reaction could not be explained by this calculation. To study the characteristics of σ_m/σ_g associated with the preequilibrium process, measurements in an extended bombarding energy range, and a further theoretical approach including the angular momentum effect are needed.

In the (p,pn) reaction, cross sections and σ_m/σ_g ratios are reproduced by the calculation only near the thresholds. The recoil-ion ranges observed for the (p,pn)^{196}Au^m indicate that this reaction proceeds through the process of the full linear momentum transfer as shown in Fig. 5, and the cross section agrees within a factor of 2~3 with the statistical-model calculation in the energy region examined here. To produce the high-spin state ($J^\pi=12^-$), a large angular momentum transfer from the incident particle to the target nucleus is apparently required because of the large difference in spin between the high spin of the product and that of the target nucleus ^{197}Au ($J^\pi=\frac{3}{2}^+$). From the single neutron states predicted by the shell model, it is unlikely that the formation of the high-spin state results from a one-step neutron pickup or knockout reaction. Therefore, it is reasonable to conclude that the nuclide ^{196}Au^m from the (p,pn) reaction is mainly produced through the compoundlike reaction. The cross sections of other reactions via charged particle emissions were not reproduced (Figs. 4, 6, and 7) by the calculation.

C. Relationship between angular momentum in the entrance channel and isomeric yield ratio

In Figs. 10(a) and 10(b), relationships between the isomeric yield ratio and the root-mean-square orbital angular momentum l_{rms} in the entrance channel are shown. The σ_m/σ_g ratios of the (d,2n) and (t,3n) reactions in Fig. 10(a) are taken from Ref. 55, as mentioned above. The l_{rms} was calculated by the optical-model and parabolic-potential subroutines of the ALICE code.[56] In Fig. 10(a), the isomeric yield ratios σ_m/σ_g are plotted for both the spin pairs of $\frac{13}{2}^+-\frac{1}{2}^-$ and 7^+-2^-. The figure shows that the observed isomeric yield ratios are strongly dependent on l_{rms} and not much on the number of neu-

tron emitted, the final nuclide, and the spin difference of the isomeric pairs. The deviation from the general trend for the σ_m/σ_g ratio in the $(p,3n)$ reaction at larger l_{rms} is ascribed to the nonequilibrium process, the occurrence of which is revealed in the recoil-ion range shown in Fig. 1. The similar behavior for the $(d,2n)$ reaction at larger l_{rms} may also be related to the same reason. In Fig. 10(b) are plotted the isomeric yield ratios observed in the reactions accompanied by charged particle emission. The σ_m/σ_g ratios for the (p,pn) and $(\alpha,\alpha n)$ reactions seem to exhibit a dependence on l_{rms} similar to those for the compoundlike reactions, but the σ_m/σ_g ratios are less than one fiftieth of the latter when compared for the same l_{rms}. This observation together with the results of the recoil-ion range for the $(p,pn)^{196}$Au^g and $(\alpha,\alpha n)^{196}$Au^{m,g} reactions reveals that those reactions are nonequilibrium processes with only a little angular momentum transfer. The isomeric yield ratios in the $(^3\text{He},\alpha)$ reaction exhibit no l_{rms} dependence, which is completely different from those of other reactions. Judging from the small isomeric yield ratios in Fig. 10(b) compared with those in Fig. 10(a), it is concluded that in the former reactions [Fig. 10(b)] the residual nuclei are formed with low angular momenta after the nonequilibrium or directlike emission of particles.

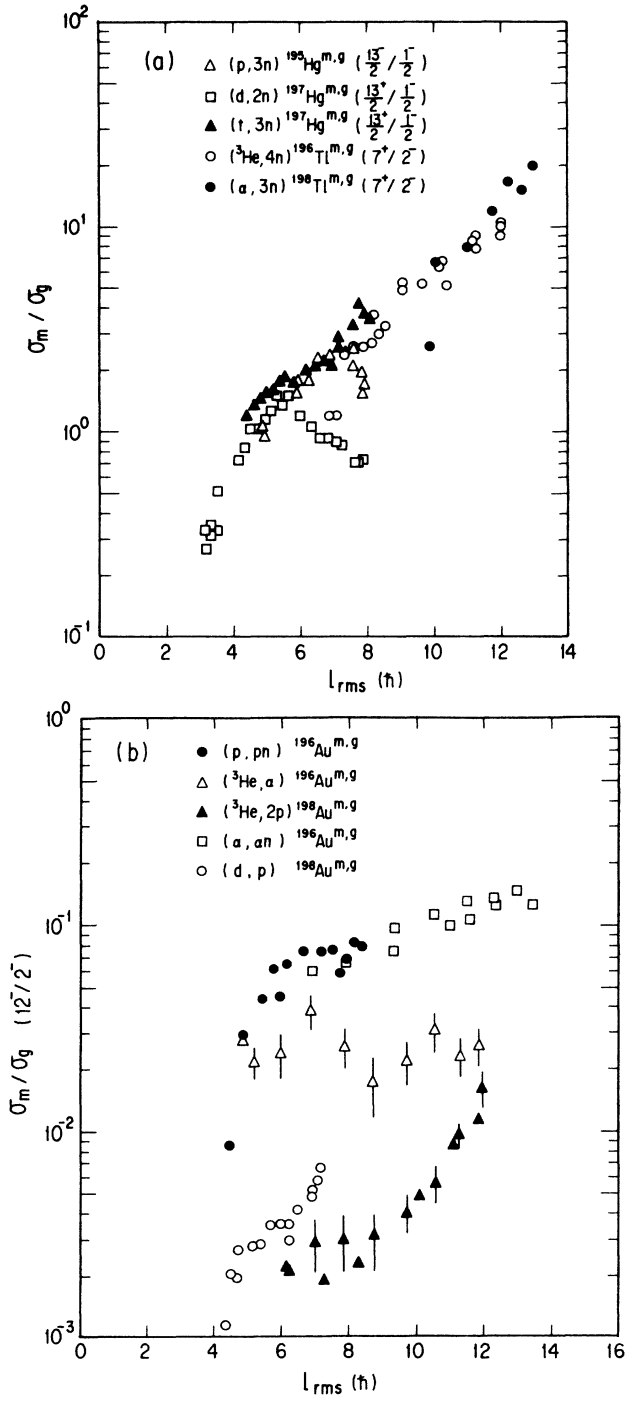

FIG. 10. Relationship between isomeric yield ratios and the root mean square orbital angular momentum l_{rms} in the entrance channel: (a) $\sigma_m/\sigma_g = \frac{13}{2}^+/\frac{1}{2}^-$ and $7^+/2^-$ vs l_{rms}, and (b) $\sigma_m/\sigma_g = 12^-/2^-$ vs l_{rms}. The l_{rms} was calculated by using the optical-model subroutines of the ALICE code.[56]

Since the isomeric yield ratios in the compoundlike reactions [Fig. 10(a)] are strongly dependent on the spin distribution of the compound nucleus as discussed above, an attempt has been made to see how the initial spin distribution is divided to reproduce the observed isomeric yield ratios. This kind of approach is useful for predicting isomeric yield ratios without executing any complicated calculation including the effect of angular momentum in the deexcitation process of particle and γ-ray emissions. Taking a sharp dividing line at $l = l_{div}$ in the initial spin distribution, and assuming that compound nuclei formed with $l \geq l_{div}$ lead to the formation of the high-spin isomer while those with $l \leq l_{div}$ give the low-spin isomer (Fig. 11). In Fig. 11 are plotted the observed isomeric yield ratios versus the sums of the partial cross sections σ_l with $l \geq |J_m - J_t|$ relative to the total reaction cross sections σ_R, where J_m and J_t are the spin of the high-spin isomer and that of the target nucleus, respectively. The solid curves show the ratio of the sum of partial cross sections between the high-spin region and the low-spin region:

$$\sum_{l=l_{div}}^{\infty} \sigma_l \Big/ \sum_{l=0}^{l_{div}} \sigma_l ,$$

where $l_{div} = |J_m - J_t| - \Delta l$ with an empirically determined parameter Δl. The data points and the solid curves do not necessarily show the same dependence on the abscissa value, but it is noticeable that the solid curves are sensitively dependent on the set of the angular momentum window, especially in the region of small and large abscissa values. The standard deviation of the observed σ_m/σ_g ratios from the solid line with $\Delta l = 1$ is 0.16 in terms of

$$\log \left[(\sigma_m/\sigma_g)_{obs} \Big/ \left[\sum_{l=l_{div}}^{\infty} \sigma_l \Big/ \sum_{l=0}^{l_{div}} \sigma_l \right] \right] .$$

This means that the isomeric yield ratios observed for the ^{197}Au target can be predicted within a factor of 0.7 to 1.4 by considering simply the spin distribution of the compound nucleus.

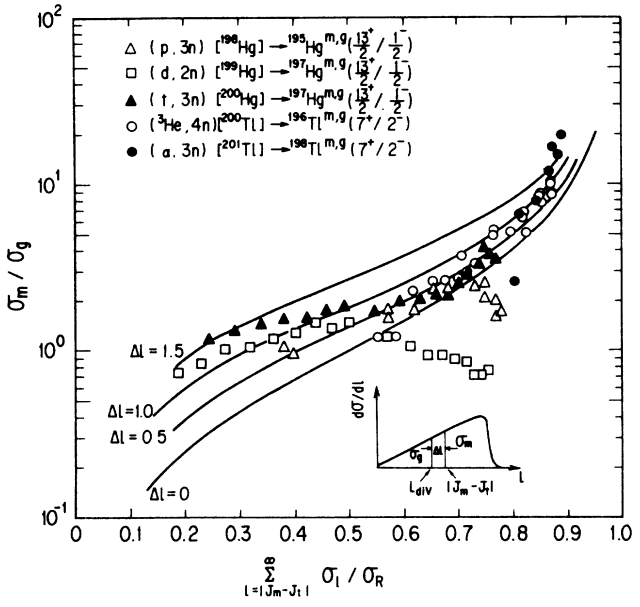

FIG. 11. Relationship between isomeric yield ratios and the sum of the partial cross sections σ_l with $l \geq |J_m - J_t|$ relative to the total reaction cross section σ_R, where J_m and J_t are the spin of the high-spin isomer and that of the target nucleus, respectively. The solid curves show the ratios of the sum of the partial cross sevtions of the high-spin region and that of the low-spin region for various Δl. In the inset, the partial cross sections for the high-spin and low-spin are schematically illustrated as a function of the compound nucleus spin l. The data for the ^{197}Au+d and ^{196}Au+t reactions are taken from Ref. 55.

V. SUMMARY AND CONCLUSION

Excitation functions and mean recoil-ion ranges of the isomeric residual nuclei in the reactions of ^{197}Au+p, ^{3}He, and α at incident energies $E_p \lesssim 50$ MeV, and $E_{^3\mathrm{He},\alpha} \lesssim 40$ MeV have been measured. The general features of the excitation functions and isomeric yield ratios were explained based on the theory of the compound nuclear reaction for the $(p,3n)$, $(^3\mathrm{He},4n)$, $(\alpha,3n)$, and $(p,pn)^{196}\mathrm{Au}^m$ reactions. On the other hand, the cross sections for the other reactions through the charged particle emissions could not be explained in the same manner. Comparison of the experimental σ_m/σ_g values between various reactions showed that there was a clear difference between the compound nuclear reaction and the direct reaction. The reactions examined here were able to be divided into three groups: (i) compoundlike reaction for the $(p,3n)$, $(^3\mathrm{He},4n)$, $(\alpha,\alpha n)$, and $(p,pn)^{196}\mathrm{Au}^m$; (ii) direct neutron transfer reaction for the $(^3\mathrm{He},2p)$; and (iii) reaction with a small angular momentum transfer for the $(p,pn)^{196}\mathrm{Au}^g$, $(^3\mathrm{He},\alpha)$, and $(\alpha,\alpha n)$. We have proposed a simple method for estimation of isomeric yield ratios from the spin distribution of the compound nucleus for the products via the compound nuclear reaction.

ACKNOWLEDGMENTS

The authors are indebted to Prof. M. Uhl for providing the statistical model computer code STAPRE. We also wish to acknowledge Dr. I. Kohno, and the crew of the RIKEN and INS cyclotrons for the accelerator operation.

[1]J. R. Huizenga and R. Vandenbosch, Phys. Rev. **120**, 1305 (1960).
[2]R. Vandenbosch and J. R. Huizenga, Phys. Rev. **120**, 1313 (1960).
[3]C. T. Bishop, J. R. Huizenga, and J. P. Hummel, Phys. Rev. **135**, B401 (1964).
[4]H. Groening, K. Aleklett, K. J. Moody, P. L. McGaughey, W. Loveland, and G. T. Seaborg, Nucl. Phys. **A389**, 80 (1982).
[5]K. J. Moody and J. J. Hogan, Phys. Rev. C **34**, 899 (1986).
[6]E. A. Skakun, V. S. Batil, Yu. N. Rakivnenko, and O. A. Rastrepin, Yad. Fiz. **46**, 28 (1987) [Sov. J. Nucl. Phys. **46**, 17 (1987)].
[7]S. M. Qaim, A. Mushtaq, and M. Uhl, Phys. Rev. C **38**, 645 (1988).
[8]R. S. Tilbury and L. Yaffe, Can. J. Chem. **41**, 2634 (1963).
[9]S. Fukushima, S. Hayashi, S. Kume, H. Okamura, K. Otozai, K. Sakamoto, and Y. Yoshizawa, Nucl. Phys. **41**, 275 (1963).
[10]S. Fukushima, S. Kume, H. Okamura, K. Otozai, K. Sakamoto, Y. Yoshizawa, and S. Hayashi, Nucl. Phys. **69**, 273 (1965).
[11]I. S. Grant and M. Rathle, J. Phys. G **5**, 1741 (1979).
[12]P. Misaelides and H. Münzel, J. Inorg. Nucl. Chem. **42**, 937 (1980).
[13]L. T. Auler, A. G. Da Silva, and G. W. A. Newton, J. Inorg. Nucl. Chem. **43**, 2611 (1981).
[14]G. W. A. Newton, V. J. Robinson, and E. M. Shaw, J. Inorg. Nucl. Chem. **43**, 2227 (1981).
[15]C. L. Branquinho, S. M. A. Hoffmann, G. W. A. Newton, V. J. Robinson, H.-Y. Wang, I. S. Grant, and J. A. B Goodall, J. Inorg. Nucl. Chem. **41**, 617 (1979).
[16]J. -P. Didelez, R. M. Lieder, H. Beuscher, D. R. Haenni, H. Machner, M. Müller-Veggian, and C. Mayer-Böricke, Nucl. Phys. **A341**, 421 (1980).
[17]H. H. Bissem, R. Georgi, W. Scobel, J. Ernst, M. Kaba, J. Rama Rao, and H Strohe, Phys. Rev. C **22**, 1468 (1980).
[18]H. H. Bissem and W. Scobel, Nukleonika **27**, 239 (1982).
[19]M. Marten, A. Schuring, W. Scobel, and H. J. Probst, Z. Phys. A **322**, 93 (1985).
[20]I. N. Vishnevskil, V. A. Zheltonozhskil, and T. N. Lashko, Yad. Fiz. **41**, 1435 (1985) [Sov. J. Nucl. Phys. **41**, 910 (1985)].
[21]H. I. West, Jr., R. G. Lanier, and M. G. Mustafa, Phys. Rev. C **35**, 2067 (1987).
[22]P. G. Young and E. D. Arthur, Los Alamos National Laboratory Report No. LA-6947, 1977.
[23]M. Uhl, in Proceedings of the Consultants Meeting on the Use of Nuclear Theory in Neutron Evaluation, Vienna, 1976, IAEA Report No. IAEA-190, p. 361; B. Strohmaier and M. Uhl, International Center for Theoretical Physics Report No. IAEA-SMR-43, 1980; B. Strohmaier, Ann. Nucl. Energy **9**,

397 (1982).
[24]C. F. Williamson, J. P. Boujot, and J. Picard, Saclay Report No. CEA-R 3042, 1966.
[25]H. L. Smith, Los Alamos National Laboratory Report No. LA-1721, 1975.
[26]W. W. Bowman and K. W. MacMurdo, At. Data Nucl. Data Tables **13**, 89 (1974).
[27]*Table of Isotopes, 7th ed.*, edited by C. M. Lederer and V. S. Shirley (Wiley, New York, 1978).
[28]J. J. Griffin, Phys. Rev. Lett. **17**, 478 (1966).
[29]M. Blann, Annu. Rev. Nucl. Sci. **25**, 123 (1975), and references therein.
[30]W. Hauser and H. Feshbach, Phys. Rev. **87**, 336 (1952).
[31]D. Wilmore and P. E. Hodgson, Nucl. Phys. **55**, 673 (1964).
[32]J. J. H. Menet, E. E. Gross, J. J. Malanify, and A. Zucker, Phys. Rev. C **4**, 1114 (1971).
[33]F. D. Becchetti, Jr. and G. W. Greenless, in *Polarization Phenomena in Nuclear Reactions*, edited by H. H. Barshall and W. Haeberli (University of Wisconsin Press, Madison, 1971), p. 682.
[34]L. Mcfadden and G. R. Satchler, Nucl. Phys. **84**, 177 (1966).
[35]G. A. Bartholomew, E. D. Earle, A. J. Ferguson, J. W. Knowless, and M. A. Lone, *Advances in Nuclear Physics* (Plenum, New York, 1973), Vol. 7, Chap. 4.
[36]J. M. Blatt and V. F. Weisskopf, *Theoretical Nuclear Physics* (Wiley, New York, 1952), p. 627.
[37]A. H. Wapstra and G. Audi, Nucl. Phys. A **432**, 1 (1985).
[38]R. L. Auble, Nucl. Data Sheets **40**, 301 (1983); H. Halperin, *ibid.* **28**, 485 (1979); B. Harmatz, *ibid.* **23**, 607 (1978).
[39]D. W. Lang, Nucl. Phys. **77**, 545 (1966).
[40]A. Gilbert and A. G. W. Cameron, Can. J. Phys. **43**, 1446 (1965).
[41]W. Dilg, W. Schantl, H. Vonach, and M. Uhl, Nucl. Phys. **A217**, 269 (1973).
[42]C. Kalbach-Cline, Nucl. Phys. **A210**, 590 (1973).
[43]Y. Nagame, Y. Nakamura, M. Takahashi, K. Sueki, and H. Nakahara, Nucl. Phys. **A486**, 77 (1988).
[44]F. C. Williams, Jr., Nucl. Phys. **A166**, 231 (1971).
[45]C. K. Cline, Nucl. Phys. **A195**, 353 (1972).
[46]M. G. Mustafa, H. I. West, Jr., H. O'Brien, R. G. Lanier, M. Benhamou, and T. Tamura, Phys. Rev. C **38**, 1624 (1988).
[47]G. M. Braga-Marcazzan, E. Gadioli-Erba, L. Milazzo-Colli, and P. G. Sona, Phys. Rev. C **6**, 1398 (1972).
[48]J. Lindhard, M. Schaff, and H. E. Schiott, Mat. Fys. Medd. Dan. Vid. Selsk. **33**, No. 14 (1963).
[49]K. Miyano and H. Nakahara, J. Phys. Soc. Jpn. **35**, 953 (1973).
[50]F. Hermes, E. W. Jasper, H. E. Kurz, T. Mayer-Kuckuk, P. F. A. Goudsmit, and H. Arnold, Nucl. Phys. **A228**, 175 (1974).
[51]O. Bousshid, Kernforschungsanlage Jülich GmbH Report No. Jül-Spez-98, 1981.
[52]F. M. Lanzafame and M. Blann, Nucl. Phys. **A142**, 545 (1970).
[53]H. E. Kurz, E. W. Jasper, K. Fischer, and F. Hermes, Nucl. Phys. **A168**, 129 (1971).
[54]N. L. Singh, A. V. Mohan Rao, S. Mukherjee, R. Upadhyay, R. K. Jain, S. K. Bose, L. Chaturvedi, and J. Rama Rao, J. Phys. G **14**, 931 (1988).
[55]V. R. Casella, Los Alamos National Laboratory Report No. LA-5830-T, 1975.
[56]M. Balnn, U. S. Energy Research and Development Administration Report Nos. COO-3494-29 and COO-3494-32, 1976.